

# Characterizing Structural Regularities of Labeled Data in Overparameterized Models

**Ziheng Jiang**<sup>\*†</sup>  
University of Washington  
ziheng@cs.washington.edu

**Chiyuan Zhang**<sup>\*</sup>  
Google Research, Brain Team  
chiyuan@google.com

**Kunal Talwar**<sup>‡</sup>  
Apple  
kunal@kunaltalwar.org

**Michael C. Mozer**  
Google Research, Brain Team  
mcmozer@google.com

## Abstract

Human learners appreciate that observations usually form hierarchies of regularities and sub-regularities. For example, English verbs have irregular cases that must be memorized (e.g.,  $GO \rightarrow WENT$ ) and regular cases that generalize well (e.g.,  $KISS \rightarrow KISSED$ ,  $MISS \rightarrow MISSED$ ). Likewise, deep neural networks have the capacity to memorize rare or irregular forms but nonetheless generalize across instances that share common patterns or structures. We analyze how individual instances are treated by a model via a *consistency score*. The score is the expected accuracy of a particular architecture for a held-out instance on a training set of a given size sampled from the data distribution. We obtain empirical estimates of this score for individual instances in multiple data sets, and we show that the score identifies out-of-distribution and mislabeled examples at one end of the continuum and regular examples at the other end. We explore two categories of proxies to the consistency score: pairwise distance based proxy and the training statistics based proxies. We conclude with two applications using C-scores to help understand the dynamics of representation learning and filter out outliers, and discussions of other potential applications such as curriculum learning, and active data collection.

## 1 Introduction

Human learning requires both inferring regular patterns that generalize across many instances and memorizing irregular examples. And the boundary regular and irregular examples can be fuzzy. For example, in learning the past tense form of English verbs, there are some verbs whose past tenses must simply be memorized ( $GO \rightarrow WENT$ ,  $EAT \rightarrow ATE$ ,  $HIT \rightarrow HIT$ ) and there are many *regular* verbs that obey the rule of appending “ed” ( $KISS \rightarrow KISSED$ ,  $KICK \rightarrow KICKED$ ,  $BREW \rightarrow BREWED$ , etc.). Generalization to a novel word typically follows the “ed” rule, for example,  $BINK \rightarrow BINKED$ . Intermediate between the exception verbs and regular verbs are subregularities—a set of exception verbs that have consistent structure (e.g., the mapping of  $SING \rightarrow SANG$ ,  $RING \rightarrow RANG$ ). Note that rule-governed and exception cases can have very similar forms, which increases the difficulty of learning each. Consider one-syllable verbs containing ‘ee’, which include the regular cases  $NEED \rightarrow NEEDED$  as well as exception cases like  $SEEK \rightarrow SOUGHT$ . Generalization from the rule-governed cases can hamper the learning of the exception cases and vice-versa. Indeed, children learning English initially master high frequency exception verbs such as  $GO \rightarrow WENT$ , but after accumulating experience with regular verbs, they begin to over-regularize by mapping  $GO \rightarrow GOED$ , eventually learning the distinction between the regular and exception verbs; neural nets show the same interesting pattern over the course of training [22].

---

<sup>\*</sup>Equal contribution.

<sup>†</sup>Work done while interning at Google.

<sup>‡</sup>Work done while at Google.

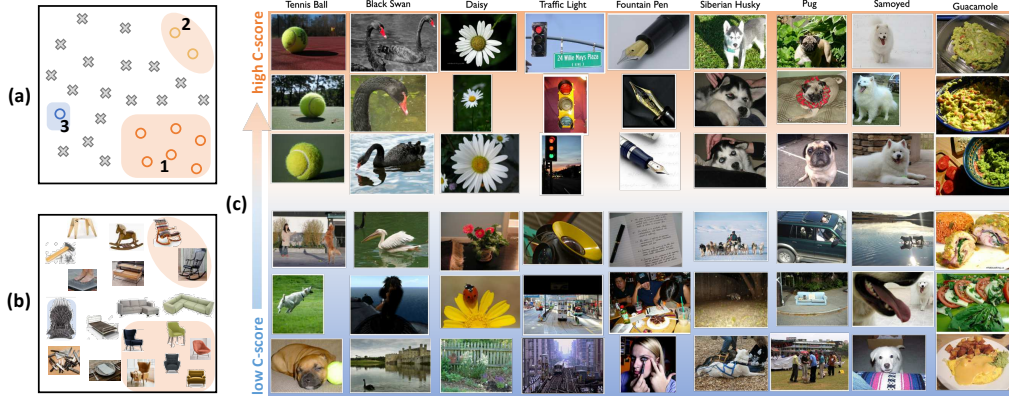


Figure 1: Regularities and exceptions in (a) a two-class input space and (b) in a latent space with chairs and non-chairs. (c) Regularities (high C-scores) and exceptions (low C-scores) in ImageNet.

Memorizing irregular examples is tantamount to building a look-up table with the individual facts accessible for retrieval. Generalization requires the inference of statistical regularities in the training environment, and the application of procedures or rules for exploiting the regularities. In deep learning, memorization is often considered a failure of a network because memorization implies no generalization. However, mastering a domain involves knowing when to generalize and when not to generalize. Consider the two-class problem with training examples positioned in an input space as in Figure 1a, or positioned in a latent space as in Figure 1b. Instance 3 (the iron throne) is an exception case and there may not exist similar cases in the data environment. Instance 1 (a generic chair) lies in a region with a consistent labeling and thus seems to follow a strong regularity. Instance 2 (a rocking chair) has a few supporting neighbors, but it lies in a distinct neighborhood from the majority of same-label instances; its neighborhood might be considered a weak regularity.

In this article, we formalize the continuum of regularities-to-exceptions in the context of a deep net. We propose a *consistency score* or *C-score* for an instance  $x$  with label  $y$ , defined as the expected accuracy of predicted label  $\hat{y}$  from a classifier of architecture  $\mathcal{A}$  trained on  $n$  i.i.d. examples drawn from a data distribution  $\mathcal{P}$ :

$$C_{\mathcal{A}, \mathcal{P}, n}(x, y) = \mathbb{E}_{D \sim \mathcal{P}} [\mathbb{P}(\hat{y}_{\mathcal{A}} = y | D, x)]. \quad (1)$$

Practically, we require that the instance  $x$  is excluded from the training set, but under a continuous data distribution, the probability of selecting the same instance for both training and testing is zero. The C-score reflects the consistency the instance is with respect to the training set: in Figure 1a, instance 1 should have a higher C-score than instance 2 which in turn should have a higher C-score than instance 3. The C-score reflects the relationship of each instance to the training population. A low C-score indicates that the instance is not aligned with the training population and therefore learning requires memorization. A high C-score indicates that the instance is supported by the training population and generalization thus follows naturally.

For a nearest-neighbor classifier that operates on the input space (Figure 1a), the C-score is related to the literature on outlier detection [8, 21, 9]. However, for a deep network, which operates over a latent space (Figure 1b), the C-score depends not just on the training data distribution but on the model architecture, loss function, optimizer, and hyperparameters. Our work is thus related to adversarial methods to identify outliers in latent space [15, 19, 3].

The C-score has many potential uses. First, it can assist in understanding a dataset’s structure by teasing apart distinct regularities and subregularities. Second, it can be used for detecting out-of-distribution and mislabeled instances: these instances will have low C-scores because they have little support from the training distribution, like instance 3 in Figure 1a. Third, it can be used to guide active data collection to improve performance of rare cases that the model treats as exceptions. Fourth, it can be used to prioritize training instances, along the lines of curriculum learning [7, 23].

There are many reasons why the C-score in Equation 1 cannot be computed. The underlying data distribution is not known. The expectation must be approximated by sampling. Each sample requires model training. Thus, we seek computationally efficient proxies for the C-score. Ideally the score could be obtained from an untrained network or a single network early in the time course of training.

In our work, we estimate a ground-truth C-score for a dataset via holdout performance on trained networks. Figure 1c shows examples of various ImageNet classes with low and high estimated C-scores. Given these

estimates, we investigate various proxies to the C-score which include measures based on: density estimation (in input, latent, and gradient spaces), and the time course of learning within a single training run. Our key contributions are as follows.

- We obtain empirical estimates of the C-score for individual instances in MNIST, CIFAR-10, CIFAR-100, and ImageNet. Estimation requires training up to 20,000 network replications per data set, permitting us to sort instances into those satisfying strong regularities, those satisfying weaker regularities, and exception (outlier) cases.
- Because empirical estimation of the C-score is computationally costly, we define and evaluate a set of candidate C-score proxies. We identified lightweight proxy scores based on the training statistics that correlates strongly ( $\rho \approx .9$ ) with the C-score and can be computed for free for all instances in the training set. We note that this result is nontrivial because the C-score is defined for held-out instances, whereas the proxy scores are defined over a training set.
- We explore two applications of the C-score to help understand the dynamics of representation learning and detect outliers, and release the estimated C-scores on ImageNet and CIFAR to foster future research and applications (see Appendix H).

## 2 Related Work

Comparing the training of Random Forests and SVMs to deep networks, [18] found that nets prioritize examples that are learnable by shallow models. Studying gradient-based learning algorithms on noise vs. real data, [2] found that with *carefully tuned* explicit regularization, a network’s capability of memorizing noisy data can be effectively controlled without compromising the generalization performance on real data.

In [10], measures are proposed for identifying *prototypical* examples which could serve as a proxy for the complete data set and still achieve good performance. These examples are not necessarily the center of a dense neighborhood, which is what our high C-score measures. Two prototype measures explored in [10], *model confidence* and the *learning speed*, are also measures we examine. Their *holdout retraining* and *ensemble agreement* metrics are conceptually similar to our holdout procedures. However, their retraining is a two-stage procedure involving pre-training and fine-tuning; their ensemble agreement mixes architectures with heterogeneous capacities and ignores labels.

[11] constructed a theoretical model showing that memorization is necessary for optimal learning when the data follows a long tail distribution. In order to quantify memorization, they defined a memorization score for each example  $(x, y)$  in a training set as the drop in prediction accuracy on  $x$  when  $(x, y)$  is removed. Our C-score closely resemble the second term of their score. With the goal of properly characterizing memorization, both terms are needed in their score. On the other hand, aiming to quantify the regularity structures of the data, we only care about the second term. Moreover, instead of leaving-*one*-out with respect to the full training set, our C-score is defined relative to reference datasets of varying size  $n$ , with a focus on understanding how the score grows with  $n$ . As we will see in Section 3, the profile of how (1) changes with gradually increasing  $n$  turns out to be very important for our purpose. Our C-score estimation procedure is built upon the estimator in [12], which empirically verified the theory from [11]. Another line of recent theoretical work studies *interpolation* [e.g. 4, 5, 16, 6], which means the model perfectly fits the training data. It is shown that in some cases interpolation is harmless for optimal generalization. Note interpolation does not necessarily imply memorization (consider fitting a linear classifier on two classes with well separated clusters).

## 3 Empirical Estimation of the C-score

Computing the C-score by Equation 1 is not feasible in practice because the underlying data distribution is typically unknown, and even if it were, the expectation cannot be computed analytically. In practice, we usually have a fixed data set  $\hat{D}$  consisting of  $N$  i.i.d. samples from the underlying distribution; for example, with the CIFAR-10 image classification task, we have 50,000 training examples. An estimate of the C-score can be computed by replacing the expectation in (1) with empirical averaging and by sampling i.i.d. subsets of a given size  $n$  from the fixed data set. We thus define the *empirical C-score* for an instance  $(x, y)$ , based on the estimator of memorization score from [11] proposed in [12]:

$$\hat{C}_{\mathcal{A}, \hat{D}, n}(x, y) = \hat{\mathbb{E}}_{D \sim \hat{D} \setminus \{(x, y)\}}^r [\mathbb{P}(\hat{y}_{\mathcal{A}} = y | D, x)], \quad (2)$$

where  $D$  is a subset of size  $n$  uniformly sampled from  $\hat{D}$  excluding  $(x, y)$ , and  $\hat{\mathbb{E}}^r$  denotes empirical averaging with  $r$  i.i.d. samples of such subsets. Because of the cost of computing  $\hat{C}$  for individual  $(x, y)$  is prohibitive,

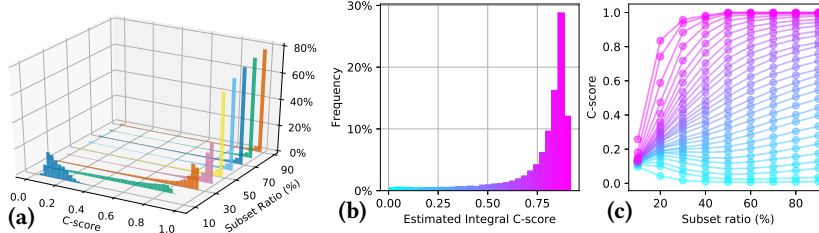


Figure 2: (a) C-score histogram for CIFAR-10 by subset ratio. (b) histogram of estimated integral C-scores for CIFAR-10. (c) C-scores by histogram bin as a function of subset ratio  $s$ . Monotonic ordering independent of  $s$ .

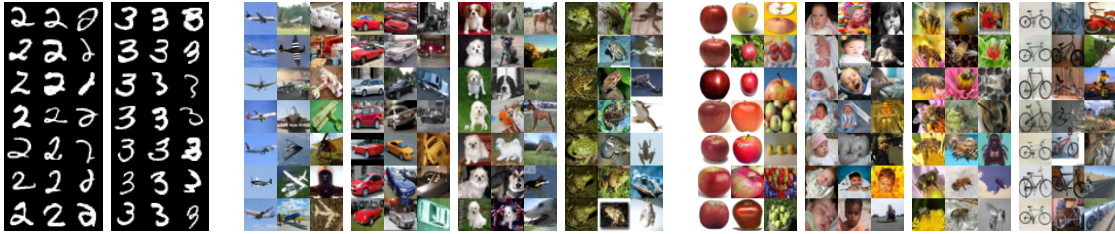


Figure 3: Examples from MNIST (blocks 1, 2), CIFAR-10 (blocks 3-6), and CIFAR-100 (blocks 7-10). Each block shows a single class; the left, middle, and right columns of a block depict instances with high, intermediate, and low C-scores, respectively.

we instead use a  $k$ -fold validation procedure. Specifically, we evaluate each fold on the  $N - n$  instances not considered for training, and determine the empirical C-score for a given instance using only the folds in which the instance is in the held-out set. We refer to this procedure as *holdout validation* (see Algorithm 1 in the Appendix).

Because each data set is a different size and we require  $n < N$ , we find it convenient to refer not to the absolute number of examples,  $n$ , but to the percentage  $s \triangleq 100n/N$  of  $\hat{\mathcal{D}}$  used for training, which we refer to as the *subset ratio*, with  $s \in [0, 100)$ . We use a 3-layer fully connected network for MNIST, Inception for CIFAR-10 / CIFAR-100 and ResNet-50 for ImageNet. Please refer to Appendix A for the full details on architectures and hyper-parameters.

Figure 2a shows the distribution of CIFAR-10 empirical C-scores for  $s \in \{10, \dots, 90\}$ . For each level of  $s$ ,  $k = 2000$  train/evaluation folds are run. Beyond giving a sense of what fraction of the data set must be used for training to obtain good generalization, the Figure suggests that floor and ceiling effects may concentrate instances, making it difficult to distinguish them based on their C-scores if  $s$  is too small or too large (will justify shortly). Rather than determining the ‘just right’ value of  $s$ , we compute a C-score marginalized over  $s$  under a uniform distribution. The left panel of Figure 2b shows a histogram of these *estimated integral C-scores*. Although the bulk of the scores are on the high end, they are more widely distributed than in the histogram for any particular  $s$  (Figure 2a).

We stratify the instances by their integral C-score into 30 bins, as indicated by the coloring of the bars of the histogram in Figure 2b. In the right panel of the Figure, we separately plot the mean C-score for the instances in a bin as a function of the subset ratio  $s$ . Note that the monotonic ordering of C-scores does not vary with  $s$ , but instances bunch up at low C-scores for small  $s$  and at high C-scores for larger  $s$ , indicated by the opacity of the open circles in the Figure. (The semi-transparent circles become opaque when superimposed on one another.) Bunching makes the instances less discriminable. At the low end of the integrated C-scores (cyan lines), note that the curves drop *below* chance (0.1 for CIFAR-10) with increasing  $s$ . We conjecture that these instances are ambiguous (e.g., visually similar to instances from a different class), and as the data set grows, regularities in other classes systematically pull these ambiguous instances in the wrong direction. This behavior is analogous to the phenomenon we mentioned earlier that children increase their production of verb overregularization errors (GO  $\rightarrow$  GOED) as they acquire more exposure to a language.

For MNIST, CIFAR-10, and CIFAR-100, Figure 3 presents instances that have varying estimated integral C-scores. Each block of examples is one category; the left, middle, and right columns have high, intermediate, and low C-scores, respectively. The homogeneity of examples in the left column suggests a large cluster of very similar images that form a functional prototype. In contrast, many of the examples in the right column are ambiguous or even mislabeled.

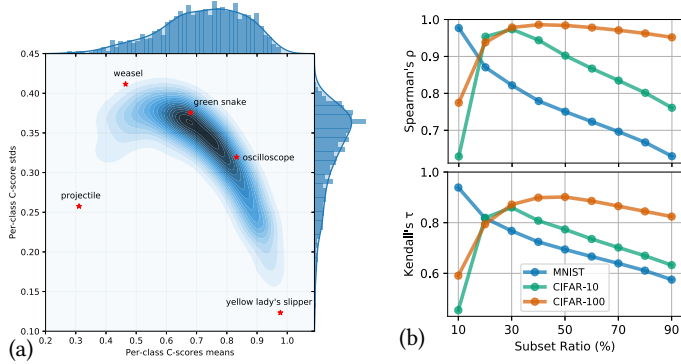


Figure 4: (a) Joint distribution of C-score per-class means and standard deviations on ImageNet. Samples from representative classes ( $\star$ 's) are shown in Figure 5. (b) Rank correlation between integral C-score and the C-score for a particular subset ratio,  $s$ . The peak of each curve indicates the training set size that best reveals generalization of the model.

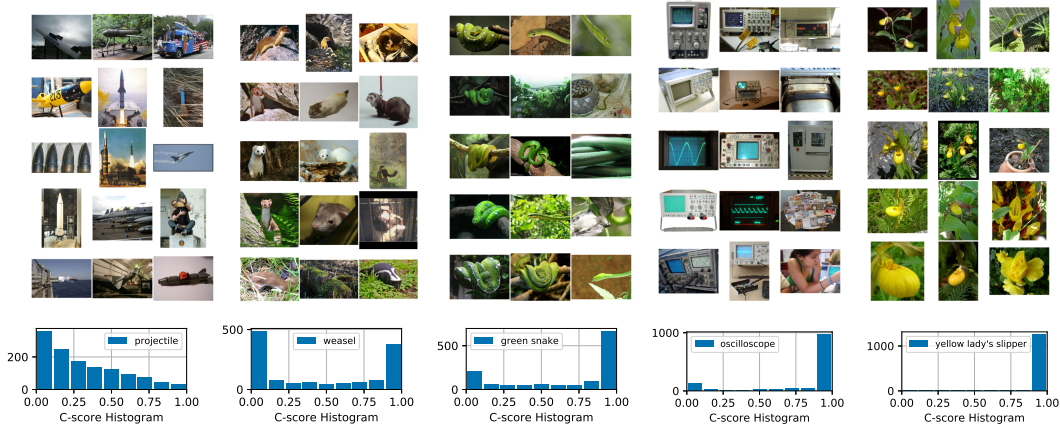


Figure 5: Example images from ImageNet. The 5 classes are chosen to have representative per-class C-score mean–standard-deviation profiles, as shown in Figure 4a. For each class, the three columns show sampled images from the (C-score ranked) top 1%, 35% and 99% percentiles, respectively. The bottom pane shows the histograms of the C-scores in each of the 5 classes.

### 3.1 Point Estimation of Integral C-score

The integral estimation computed in the previous section requires invoking the holdout validation procedure for a range of  $s$ , with each invocation involving training on the order of 2000 networks. For large-scale data sets like ImageNet, the computational cost of this approximate integration is too high. Consequently, we investigate the feasibility of approximating the integral C-score with a *point estimate*, i.e., selection of the  $s$  that best represents the integral score. By ‘best represents,’ we mean that the ranking of instances by the integral score matches the ranking by the score for a particular  $s$ . Figure 4b shows rank correlation between integral score and score for a given  $s$ , as a function of  $s$ . Each curve in the graph corresponds to a particular data set. Examining the green CIFAR-10 curve, there is a peak at  $s = 30$ , indicating that  $s = 30$  yields the best point-estimate approximation for the integral C-score. That the peak is at an intermediate  $s$  is consistent with the observation from Figure 2b that the C-score bunches together instances for low and high  $s$ .

For MNIST, a less challenging data set than CIFAR-10, the peak is lower, at  $s = 10$ ; for CIFAR-100, a more challenging data set than CIFAR-10, the peak is higher, at  $s = 40$  or  $s = 50$ . Thus, the peak appears to shift to larger  $s$  for more challenging data sets. This finding is not surprising: more challenging data sets require a greater diversity of training instances in order to observe generalization.

### 3.2 ImageNet

In addition to MNIST, CIFAR-10, and CIFAR-100, we conducted experiments with ImageNet. Due to the large data set size (1.2M examples), we picked a single  $s$  for our C-score estimate. Based on the fact that the optimal  $s$  increases with data set complexity, we picked  $s = 70$  for ImageNet. In particular, we train 2,000 ResNet-50 models each with a random 70% subset of the ImageNet training set, and compute the C-scores for all the training examples.

The examples shown in Figure 1c are ranked according to this C-score estimate. Because ImageNet has 1,000 classes, we cannot offer a simple overview over the entire dataset as in MNIST and CIFAR. Thus, we focus on analyzing the behaviors of individual classes. Specifically, we compute the mean and standard deviation (SD) of the C-scores of all the examples in a particular class. The mean C-scores indicates the relative difficulty of classes, and the SD indicates the diversity of examples within each class. The two-dimensional histogram in Figure 4a depicts the joint distribution of mean and SD across all classes. A strong correlation is observed: classes with high mean C-scores tend to have low variances. We selected several classes with various combinations of mean and SD, indicated by the  $\star$ 's in Figure 4a. We then selected sample images from the top 1%, 35% and 99% percentile ranked by the C-score within each class, and show them in Figure 5.

The class *projectile* has C-scores spread out the value range. In contrast, the class *weasel* has large masses on both low and high C-scores, leading to larger variance than *projectile*. The class *green snake* from the high density region of the 2D histogram in Figure 4a represent common cases in the 1,000 ImageNet classes: while highly regular examples dominate, there are also usually a non-trivial number of outliers or ambiguous examples that need to be memorized in training. The class *oscilloscope* is similar to *green snake* except with higher mean and lower SD. On the other extreme of the spectrum is the class *yellow lady's slipper*, which mostly contain highly regular examples. From the image samples, we can see even the 99% percentile ranked examples enjoy a consistent color scheme with the rest of the images.

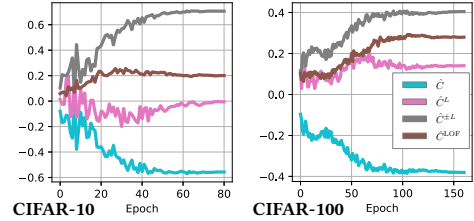


Figure 6: Spearman rank correlation between C-score and distance-based score on hidden representations.

## 4 C-Score Proxies

Given meaningful estimates of the C-score, we now investigate proxies to the C-score. To unwind the logic of our investigation, the C-score relates to the consistency of a given  $(x, y)$  instance with the rest of the data set. We’ve shown that it is useful for understanding the data set structure and for identifying outliers and mislabeled instances. However, it is expensive to estimate. Our goal in this section is to identify proxy measures strongly correlated with the C-score that can be estimated before or while a model is training *on the training instances alone*. We emphasize this latter point because if we are successful in estimating C-scores for training examples, we should also be able to estimate performance of as-yet-unseen data. We explore two C-score proxy measures based on density estimation—in input and in latent space—as well as a measure based on accuracy over the time course of training. In addition, we discuss a gradient-based measure related to the neural tangent kernel [13] in the supplementary materials (Appendix C.2). All of these measures have the property that they require training only a single instance of the model and they can be used to estimate performance on a training example without explicit holdout.

### 4.1 Proxies Based on Pairwise Distances

In this section, we study C-score proxies based on pairwise distances. Intuitively, an example is consistent with the data distribution if it lies near other examples having the same label. However, if the example lies far from instances in the same class or lies near instances of different classes, one might not expect it to generalize. Based on this intuition, we define a relative local-density score:

$$\hat{C}^{\pm L}(x, y) = \frac{1}{N} \sum_{i=1}^N 2(\mathbf{1}[y = y_i] - \frac{1}{2})K(x_i, x), \quad (3)$$

where  $K(x, x') = \exp(-\|x - x'\|^2/h^2)$  is an RBF kernel with the bandwidth  $h$ , and  $\mathbf{1}[\cdot]$  is the indicator function. To evaluate the importance of explicit label information, we study two related scores:  $\hat{C}^L$  that uses only same-class examples when estimating the local density, and  $\hat{C}$  that uses all the neighbor examples by ignoring the labels. We also study a proxy based on the local outlier factor (LOF) algorithm [8], which measures the local deviation of each point with respect to its neighbours. Since large LOF scores indicate outliers, we use the negative LOF score as a C-score proxy, denoted by  $\hat{C}^{\text{LOF}}(x)$ .

We found that proxies based on pairwise distances in the input space work poorly (see Appendix C.1). Using the penultimate layer of the network as a representation of an image, we evaluate the proxy scores:  $\hat{C}_h^{\pm L}$ ,  $\hat{C}_h^L$ ,  $\hat{C}_h$  and  $\hat{C}_h^{\text{LOF}}$ , with the subscript  $h$  indicating that the score operates in hidden space. For each score and data set, we compute Spearman’s rank correlation between the proxy score and the C-score. Because the embedding changes as the network is trained, we plot the correlation as a function of training epoch in Figure 6. For both

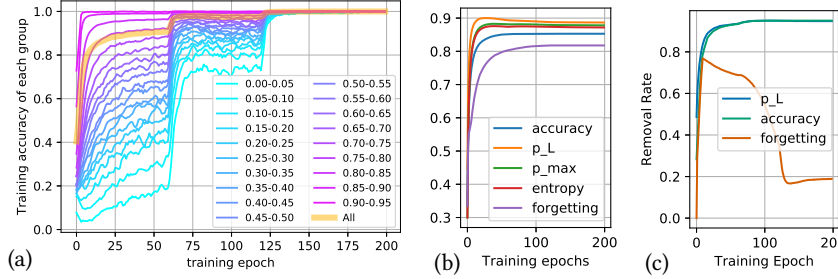


Figure 7: (a) Learning speed of groups ranked by C-scores. (b) Rank correlation (Spearman’s  $\rho$ ) between C-score and training statistics based proxies. (c) Using C-score proxies to identify outliers on CIFAR-10 (25% random label corruption).

data sets, the proxy score that correlates best with the C-score is  $\hat{C}_h^{\pm L}$  (grey), followed by  $\hat{C}_h^{\text{LOF}}$  (brown), then  $\hat{C}_h^L$  (pink) and  $\hat{C}_h$  (blue). Clearly, appropriate use of labels helps with the ranking. However, our proxy  $\hat{C}_h^{\pm L}$  uses the labels in an ad hoc manner. In Appendix C.2, we discuss a more principled measure based on gradient vectors and relate it to the neural tangent kernel [13].

Even at asymptote,  $\hat{C}_h^{\pm L}$  achieves a peak correlation of only about 0.7 for MNIST and CIFAR-10 and 0.4 for CIFAR-100. Nonetheless, the curves in Figure 6 offer an intriguing hint that information in the time course of training may be valuable for predicting the C-score. We thus investigate the time course of training itself in the next section, specifically, we examine the accuracy of an example in the training set as the network weights evolve.

## 4.2 Proxies Based on Training Statistics

Intuitively, a training example that is consistent with many others should be learned quickly because the gradient steps for all consistent examples should be well aligned. One might therefore conjecture that strong regularities in a data set are not only better learned at asymptote—leading to better generalization performance—but are also learned *sooner* in the time course of training. This *learning speed* hypothesis is nontrivial, because the C-score is defined for a held-out instance following training, whereas learning speed is defined for a training instance during training.

To test the learning-speed hypothesis, we partitioned examples in the CIFAR-10 data set into bins by integrated C-score, each bin having a width of 0.05. We then train a model on *all* examples in the data set and plot average proportion correct for each bin as a function of training epoch, as shown in Figure 7a. The two jumps in the graph correspond to points at which the learning rate is reduced. Asymptotically, all examples are learned, as one would expect from an overparameterized model. However, interestingly, the (cyan) examples having the lowest C-scores are learned most slowly and the (purple) examples having the highest C-scores are learned most quickly. Indeed, learning speed is monotonically related to C-score bin.

In Figure 7b, we compute the Spearman’s rank correlation between the C-score of an instance and a number of proxy scores based on learning speed. In particular, we test *accuracy* (0-1 correctness),  $p_L$  (softmax confidence on the correct class),  $p_{\max}$  (max softmax confidence across all classes) and *entropy* (negative entropy of softmax confidences). We use the *cumulative* statistics which average from the beginning of training to the current epoch because this result in higher correlation than using the scores based on any single epoch. We also compare to *forgetting event* [25], which is a cumulative statistics that counts the number of transitions from “learned” to “forgotten” during training.

All those proxies show strong correlation with the C-score.  $p_L$  reaches  $\rho \approx 0.9$  at the peak.  $p_{\max}$  and *entropy* perform similarly, both slightly worse than  $p_L$ . The plot also shows that examples with low cscores are more likely to be forgotten during training. However, the *forgetting event* based proxy under-performs other proxies and takes more number of training epochs to reach its peak correlation. Because forgetting events happen only after an example is learned, so unlike other proxies studied here, forgetting statistics for hard examples cannot be obtained in the earlier stage of training.

## 5 Applications

The C-score allows detailed analysis over the structural regularities of datasets that are otherwise challenging to get a succinct description of organization of data points. For example, the visualization of regular examples (Figure 3) reveals the common color and shape structures shared by many examples in each class. The analysis of the C-score distributions in different classes (Figure 4a) helps to identify individual classes that are especially

hard to learn due to extremely diverse instances. We offer two examples to show applications to downstream tasks beyond the analysis of the datasets.

First, we use C-score-based example grouping to analyze learning dynamics. In Figure 7a, we note that stagewise learning rate decay has a greater impact for examples with lower C-scores. Larger learning rates limit learning of low C-score examples. This observation suggests a plausible explanation for why we, like other computer vision researchers, have observed better generalization with stagewise than with constant learning rates. Starting with a large learning rate effectively enforces a sort of curriculum in which the model first learns the strongest regularities. At a later stage when the learning rate is lowered and exceptions or outliers are able to be learned, the model has already built a representation based on domain regularities. Detailed studies with comparison to constant learning rates are found in Appendix G, where we also provide insights to the long debating puzzle [26, 14, 17] why Adam sometimes converges faster but generalizes worse than SGD with stagewise learning rates (95.14% vs 92.97% in our case).

The second example uses C-score proxies to identify outliers. We corrupt a fraction  $\gamma$  of the CIFAR-10 training set with random label assignments. Then during training, we identify the fraction  $\gamma$  with the lowest ranking by our C-score proxies—cumulative accuracy,  $p_L$ , and forgetting-event statistics. Figure 7c shows the removal rate—the fraction of the lowest ranked examples which are indeed outliers; two of the C-score proxies successfully identify over 95% of outliers (see Figure 18 in the appendix for more results). Both examples suggest that C-scores could be useful for curriculum learning and related applications. We leave systematic exploration along this line to future work. We share the pre-computed C-scores (see Appendix H) to foster future research and applications.

## 6 Discussion

We explored the memorization-generalization continuum in deep learning via a *consistency score* that measures the statistical regularity of an instance in the context of a data distribution. We empirically estimated the C-score for individual instances in four data sets and we explored various proxies to the C-score based on density estimation and the time course of training. Our main contributions and take-home messages are as follows.

- We assign a consistency score (C-score) to every example in MNIST, CIFAR-10, CIFAR-100, and ImageNet. These scores can assist in understanding a data set’s structure by teasing apart regularities, subregularities, and exception cases. We are currently investigating whether the scores can be used to improve generalization via curriculum learning or instance reweighting, in particular, with the aim of encouraging networks to discover regularities before exceptions are memorized. The C-score can also be used to identify ambiguous and mislabeled examples for data cleaning and to identify difficult corner cases in safety critical applications for active data collection.
- High C-score instances tend to be visually uniform in color, shape, alignment (see Appendix E for more examples). Lowest C-score instances are often mislabeled or the salient object in the image belongs to a different class. In ImageNet, some classes do appear to have strong regularities, such as *yellow lady’s slipper*. However, other classes, such as *projectile*, are more notable for their extreme diversity. Diversity seems to be reflected in the intra-class C-score variance.
- The cumulative statistics based on  $p_L$  is a good proxy to the C-score. It costs almost nothing to compute and requires just one training run, not thousands like the C-score. Remarkably, the statistics is based on the *training* performance of an instance, yet it predicts ( $\rho \approx .9$ ) the C-score, which is the *generalization* performance of that same instance if it were held out of the training set.
- Tracking the learning speed of examples grouped by C-score, we formulated a hypothesis to explain why a stage-wise decreasing learning-rate schedule often generalizes better than a constant or adaptive schedule. Our analysis suggests that the stage-wise schedule provides scaffolding to build internal representations based on the strongest domain regularities first.

In the 1980s, neural nets were touted for learning *rule-governed behavior* without explicit rules [22]. At the time, AI researchers were focused on constructing expert systems by extracting explicit rules from human domain experts. Expert systems ultimately failed because the diversity and nuance of statistical regularities in a domain was too great for any human to explicate. In the modern deep learning era, researchers have made much progress in automatically extracting regularities from data. Nonetheless, there is still much work to be done to understand these regularities, and how the consistency relationships among instances determine the outcome of learning. By defining and investigating a consistency score, we hope to have made some progress in this direction.

## Acknowledgments

We thank Vitaly Feldman for guidance on simulation design and framing of the research, Samy Bengio for general comments and feedback, and Yoram Singer for making the collaboration possible.

## References

- [1] M. Abadi, A. Agarwal, P. Barham, E. Brevdo, Z. Chen, C. Citro, G. S. Corrado, A. Davis, J. Dean, M. Devin, S. Ghemawat, I. Goodfellow, A. Harp, G. Irving, M. Isard, Y. Jia, R. Jozefowicz, L. Kaiser, M. Kudlur, J. Levenberg, D. Mané, R. Monga, S. Moore, D. Murray, C. Olah, M. Schuster, J. Shlens, B. Steiner, I. Sutskever, K. Talwar, P. Tucker, V. Vanhoucke, V. Vasudevan, F. Viégas, O. Vinyals, P. Warden, M. Wattenberg, M. Wicke, Y. Yu, and X. Zheng. TensorFlow: Large-scale machine learning on heterogeneous systems, 2015. URL <https://www.tensorflow.org/>. Software available from tensorflow.org.
- [2] D. Arpit, S. Jastrzębski, N. Ballas, D. Krueger, E. Bengio, M. S. Kanwal, T. Maharaj, A. Fischer, A. Courville, Y. Bengio, et al. A closer look at memorization in deep networks. In *Proceedings of the 34th International Conference on Machine Learning-Volume 70*, pages 233–242. JMLR. org, 2017.
- [3] L. Beggel, M. Pfeiffer, and B. Bischl. Robust anomaly detection in images using adversarial autoencoders, 2019.
- [4] M. Belkin, D. J. Hsu, and P. Mitra. Overfitting or perfect fitting? risk bounds for classification and regression rules that interpolate. In *Advances in neural information processing systems*, pages 2300–2311, 2018.
- [5] M. Belkin, S. Ma, and S. Mandal. To understand deep learning we need to understand kernel learning. *arXiv preprint arXiv:1802.01396*, 2018.
- [6] M. Belkin, D. Hsu, and J. Xu. Two models of double descent for weak features. *arXiv preprint arXiv:1903.07571*, 2019.
- [7] Y. Bengio, J. Louradour, R. Collobert, and J. Weston. Curriculum learning. In *Proceedings of the 26th annual international conference on machine learning*, pages 41–48. ACM, 2009.
- [8] M. M. Breunig, H.-P. Kriegel, R. T. Ng, and J. Sander. Lof: identifying density-based local outliers. In *Proceedings of the 2000 ACM SIGMOD international conference on Management of data*, pages 93–104, 2000.
- [9] G. O. Campos, A. Zimek, J. Sander, R. J. G. B. Campello, B. Micenková, E. Schubert, I. Assent, and M. E. Houle. On the evaluation of unsupervised outlier detection: measures, datasets, and an empirical study. *Data Mining and Knowledge Discovery*, 30(4):891–927, 2016.
- [10] N. Carlini, U. Erlingsson, and N. Papernot. Prototypical examples in deep learning: Metrics, characteristics, and utility. Technical report, OpenReview, 2018.
- [11] V. Feldman. Does learning require memorization? A short tale about a long tail. In *ACM Symposium on Theory of Computing (STOC)*, 2020.
- [12] V. Feldman and C. Zhang. What neural networks memorize and why: Discovering the long tail via influence estimation. Preprint, 2020.
- [13] A. Jacot, F. Gabriel, and C. Hongler. Neural tangent kernel: Convergence and generalization in neural networks. In *Advances in neural information processing systems*, pages 8571–8580, 2018.
- [14] N. S. Keskar and R. Socher. Improving generalization performance by switching from adam to sgd. *arXiv preprint arXiv:1712.07628*, 2017.
- [15] K. Lee, K. Lee, H. Lee, and J. Shin. A simple unified framework for detecting out-of-distribution samples and adversarial attacks. In S. Bengio, H. Wallach, H. Larochelle, K. Grauman, N. Cesa-Bianchi, and R. Garnett, editors, *Advances in Neural Information Processing Systems 31*, pages 7167–7177. Curran Associates, Inc., 2018.
- [16] T. Liang and A. Rakhlin. Just interpolate: Kernel" ridgeless" regression can generalize. *arXiv preprint arXiv:1808.00387*, 2018.

- [17] L. Luo, Y. Xiong, Y. Liu, and X. Sun. Adaptive gradient methods with dynamic bound of learning rate. In *International Conference on Learning Representations*, 2019.
- [18] K. Mangalam and V. U. Prabhu. Do deep neural networks learn shallow learnable examples first? In *ICML 2019 Workshop on Identifying and Understanding Deep Learning Phenomena*, 2019.
- [19] S. Pidhorskyi, R. Almohsen, and G. Doretto. Generative probabilistic novelty detection with adversarial autoencoders. In S. Bengio, H. Wallach, H. Larochelle, K. Grauman, N. Cesa-Bianchi, and R. Garnett, editors, *Advances in Neural Information Processing Systems 31*, pages 6822–6833. Curran Associates, Inc., 2018.
- [20] A. Radford, J. Wu, R. Child, D. Luan, D. Amodei, and I. Sutskever. Language models are unsupervised multitask learners. *OpenAI Blog*, 1(8):9, 2019.
- [21] S. Ramaswamy, R. Rastogi, and K. Shim. Efficient algorithms for mining outliers from large data sets. *SIGMOD Rec.*, 29(2):427–438, May 2000. ISSN 0163-5808. doi: 10.1145/335191.335437.
- [22] D. E. Rumelhart and J. L. McClelland. *On Learning the Past Tenses of English Verbs*, page 216–271. MIT Press, Cambridge, MA, USA, 1986.
- [23] S. Saxena, O. Tuzel, and D. DeCoste. Data parameters: A new family of parameters for learning a differentiable curriculum. In H. Wallach, H. Larochelle, A. Beygelzimer, F. d’Alché-Buc, E. Fox, and R. Garnett, editors, *Advances in Neural Information Processing Systems 32*, pages 11093–11103. Curran Associates, Inc., 2019.
- [24] M. Tan and Q. V. Le. Efficientnet: Rethinking model scaling for convolutional neural networks. *arXiv preprint arXiv:1905.11946*, 2019.
- [25] M. Toneva, A. Sordoni, R. T. d. Combes, A. Trischler, Y. Bengio, and G. J. Gordon. An empirical study of example forgetting during deep neural network learning. In *International Conference on Learning Representations*, 2019.
- [26] A. C. Wilson, R. Roelofs, M. Stern, N. Srebro, and B. Recht. The marginal value of adaptive gradient methods in machine learning. In *Advances in Neural Information Processing Systems*, pages 4148–4158, 2017.

# Appendix for “Characterizing Structural Regularities of Labeled Data in Overparameterized Models”

## A Experiment Details

The details on model architectures, dataset information and hyper-parameters used in the experiments for empirical estimation of the C-score can be found in Table 1. We implement our experiment in Tensorflow [1]. The holdout subroutine used in C-score estimation is listed in Algorithm 1. Most of the training jobs for C-score estimation are run on single NVidia® Tesla P100 GPUs. The ImageNet training jobs are run with 8 P100 GPUs using single-node multi-GPU data parallelization.

To compute the scores based on kernel density estimation on learned representations, we train neural network models with the same specification as in Table 1 on the full training set. We use an RBF kernel  $K(x, x') = \exp(-\|x - x'\|^2 / h^2)$ , where the bandwidth parameter  $h$  is adaptively chosen as  $1/2$  of the mean pairwise Euclidean distance across the dataset. For the local outlier factor (LOF) algorithm [8], we use the neighborhood size  $k = 3$ . See Figure 8 for the behavior of LOF across a wide range of neighborhood sizes.

The experiments on learning speed are conducted with ResNet-18 on CIFAR-10, trained for 200 epochs while batch size is 32. For optimizer, we use the SGD with the initial learning rate 0.1, momentum 0.9 (with Nesterov momentum) and weight decay is  $5e-4$ . The stage-wise constant learning rate scheduler decrease the learning rate at the 60th, 90th, and 120th epoch with a decay factor of 0.2.

---

**Algorithm 1** Holdout validation

---

**Input:** Data set  $\hat{\mathcal{D}} = (X, Y)$  with  $N$  examples  
**Input:**  $n$ : number of instances used for training  
**Input:**  $k$ : number of folds  
**Output:**  $\hat{C} \in \mathbb{R}^N$ : C-score estimate of each example  
Initialize binary mask matrix  $M \leftarrow 0^{k \times N}$   
Initialize 0-1 loss matrix  $L \leftarrow 0^{k \times N}$   
**for**  $i \in (1, 2, \dots, k)$  **do**  
    Sample  $n$  random indices  $I$  from  $\{1, \dots, N\}$   
     $M[i, I] \leftarrow 1$   
    Train  $\hat{f}$  from scratch with the subset  $X[I], Y[I]$   
     $L[i, :] \leftarrow 1[\hat{f}(X) \neq Y]$   
**end for**  
Initialize score estimation vector  $\hat{C} \leftarrow 0^N$   
**for**  $j \in (1, 2, \dots, N)$  **do**  
     $Q \leftarrow \neg M[:, j]$   
     $\hat{C}[j] \leftarrow \text{sum}(\neg L[:, Q]) / \text{sum}(Q)$   
**end for**

---

## B Time and Space Complexity

The time complexity of the holdout procedure for empirical estimation of the C-score is  $O(S(kT + E))$ . Here  $S$  is the number of subset ratios,  $k$  is number of holdout for each subset ratio, and  $T$  is the average training time for a neural network.  $E$  is the time for computing the score given the  $k$ -fold holdout training results, which involves elementwise computation on a matrix of size  $k \times N$ , and is negligible comparing to the time for training neural networks. The space complexity is the space for training a single neural network times the number of parallel training jobs. The space complexity for computing the scores is  $O(kN)$ .

For kernel density estimation based scores, the most expensive part is forming the pairwise distance matrix (and the kernel matrix), which requires  $O(N^2)$  space and  $O(N^2d)$  time, where  $d$  is the dimension of the input or hidden representation spaces.

Table 1: Details for the experiments used in the empirical estimation of the C-score.

	MNIST	CIFAR-10	CIFAR-100	ImageNet
Architecture	MLP(512,256,10)	Inception <sup>†</sup>	Inception <sup>†</sup>	ResNet-50 (V2)
Optimizer	SGD	SGD	SGD	SGD
Momentum	0.9	0.9	0.9	0.9
Base Learning Rate	0.1	0.4	0.4	0.1×7
Learning Rate Scheduler	$\wedge(15\%)^*$	$\wedge(15\%)^*$	$\wedge(15\%)^*$	LinearRampupPiecewiseConstant <sup>**</sup>
Batch Size	256	512	512	128×7
Epochs	20	80	160	100
Data Augmentation	.....	Random Padded Cropping <sup>⊗</sup> + Random Left-Right Flipping .....		
Image Size	28×28	32×32	32×32	224×224
Training Set Size	60,000	50,000	50,000	1,281,167
Number of Classes	10	10	100	1000

<sup>†</sup> A simplified Inception model suitable for small image sizes, defined as follows:

Inception :: Conv(3×3, 96) → Stage1 → Stage2 → Stage3 → GlobalMaxPool → Linear.

Stage1 :: Block(32, 32) → Block(32, 48) → Conv(3×3, 160, Stride=2).

Stage2 :: Block(112, 48) → Block(96, 64) → Block(80, 80) → Block(48, 96) → Conv(3×3, 240, Stride=2).

Stage3 :: Block(176, 160) → Block(176, 160).

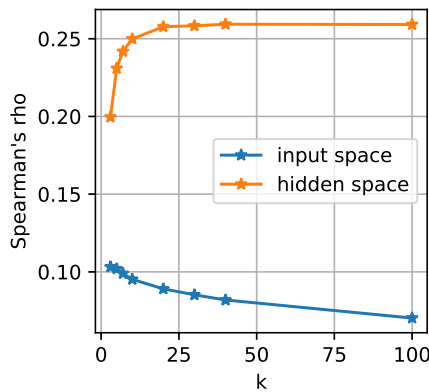
Block( $C_1, C_2$ ) :: Concat(Conv(1×1,  $C_1$ ), Conv(3×3,  $C_2$ )).

Conv :: Convolution → BatchNormalization → ReLU.

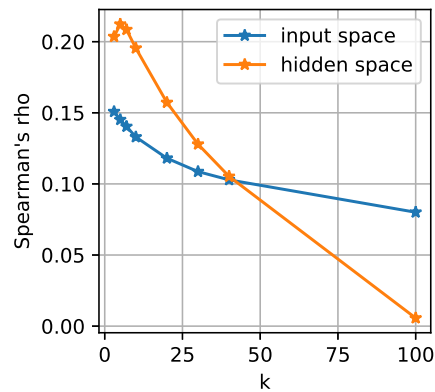
★  $\wedge(15\%)$  learning rate scheduler linearly increase the learning rate from 0 to the *base learning rate* in the first 15% training steps, and then from there linear decrease to 0 in the remaining training steps.

★★ LinearRampupPiecewiseConstant learning rate scheduler linearly increase the learning rate from 0 to the *base learning rate* in the first 15% training steps. Then the learning rate remains piecewise constant with a 10× decay at 30%, 60% and 90% of the training steps, respectively.

⊗ Random Padded Cropping pad 4 pixels of zeros to all the four sides of MNIST, CIFAR-10, CIFAR-100 images and (randomly) crop back to the original image size. For ImageNet, a padding of 32 pixels is used for all four sides of the images.



(a) CIFAR-10



(b) CIFAR-100

 Figure 8: The Spearman's  $\rho$  correlation between the C-score and the score based on LOF with different neighborhood sizes.

Table 2: Rank correlation between C-score and pairwise distance based proxies on inputs. Measured with Spearman’s  $\rho$  and Kendall’s  $\tau$  rank correlations, respectively.

		$\hat{C}$	$\hat{C}^L$	$\hat{C}^{\pm L}$	$\hat{C}^{\text{LOF}}$
$\rho$	CIFAR-10	-0.064	-0.009	0.083	0.103
	CIFAR-100	-0.098	0.117	0.105	0.151
$\tau$	CIFAR-10	-0.042	-0.006	0.055	0.070
	CIFAR-100	-0.066	0.078	0.070	0.101

## C Proxies Based on Pairwise Distances

In the studies of pairwise distance based proxies for the C-score in Section 4.1, We defined a relative local-density score  $\hat{C}^{\pm L}(x, y)$  in (3). We provided the definitions of the two related scores here. First, we define a class-conditional density score:

$$\hat{C}^L(x, y) = \frac{1}{N} \sum_{i=1}^N \mathbf{1}[y = y_i] K(x_i, x), \quad (4)$$

(Because we are mainly interested in the relative ranking of examples, we do not normalize the score to form a proper probability density function.) If  $\hat{C}^{\pm L}(x, y)$  is a better proxy than  $\hat{C}^L(x, y)$ , then the contrast between classes is critical. Second, we define a class-independent density score:

$$\hat{C}(x) = \frac{1}{N} \sum_{i=1}^N K(x_i, x). \quad (5)$$

If  $\hat{C}^L(x, y)$  is a better proxy than  $\hat{C}(x)$ , then the class labels are critical.

### C.1 Evaluations Based on Distances in the Input Space

Table 2 shows the agreement between the proxy scores and the estimated C-score. Agreement is quantified by two rank correlation measures on three data sets. As anticipated, the input-density score that ignores labels,  $\hat{C}(x)$ , and the class-conditional density,  $\hat{C}^L(x, y)$ , have poor agreement.  $\hat{C}^{\pm L}(x, y)$  and  $\hat{C}^{\text{LOF}}$  are slightly better. However, none of the proxies has high enough correlation to be useful, because it is very hard to obtain semantically meaningful distance estimations from the raw pixels.

### C.2 Pairwise Distance Estimation with Gradient Representations

Most modern neural networks are trained with first order gradient descent based algorithms and variants. In each iteration, the gradient of loss on a mini-batch of training examples evaluated at the current network weights is computed and used to update the current parameter. Let  $\nabla_t(\cdot)$  be the function that maps an input-label training pair (the case of mini-batch size one) to the corresponding gradient evaluated at the network weights of the  $t$ -th iteration. Then this defines a gradient based representation on which we can compute density based ranking scores. The intuition is that in a gradient based learning algorithm, an example is consistent with others if they all compute similar gradients.

Comparing to the hidden representations defined the outputs of a neural network layer, the gradient based representations induce a more natural way of incorporating the label information. In the previous section, we reweight the neighbor examples belonging to a different class by 0 or -1. For gradient based representations, no ad hoc reweighting is needed as the gradient is computed on the loss that has already takes the label into account. Similar inputs with different labels automatically lead to dissimilar gradients. Moreover, this could seamlessly handle labels and losses with rich structures (e.g. image segmentation, machine translation) where an effective reweighting scheme is hard to find. The gradient based representation is closely related to recent developments on Neural Tangent Kernels (NTK) [13]. It is shown that when the network width goes to infinity, the neural network training dynamics can be effectively approximately via Taylor expansion at the initial network weights. In other words, the algorithm is effectively learning a *linear* model on the *nonlinear* representations defined by  $\nabla_0(\cdot)$ . This feature map induces the NTK, and connects deep learning to the literature of kernel machines.

Although NTK enjoys nice theoretical properties, it is challenging to perform density estimation on it. Even for the more practical case of *finite width* neural networks, the gradient representations are of extremely high dimensions as modern neural networks general have parameters ranging from millions to billions [e.g. 24, 20]. As a result, both computation and memory requirements are prohibitive if a naive density estimation is to be

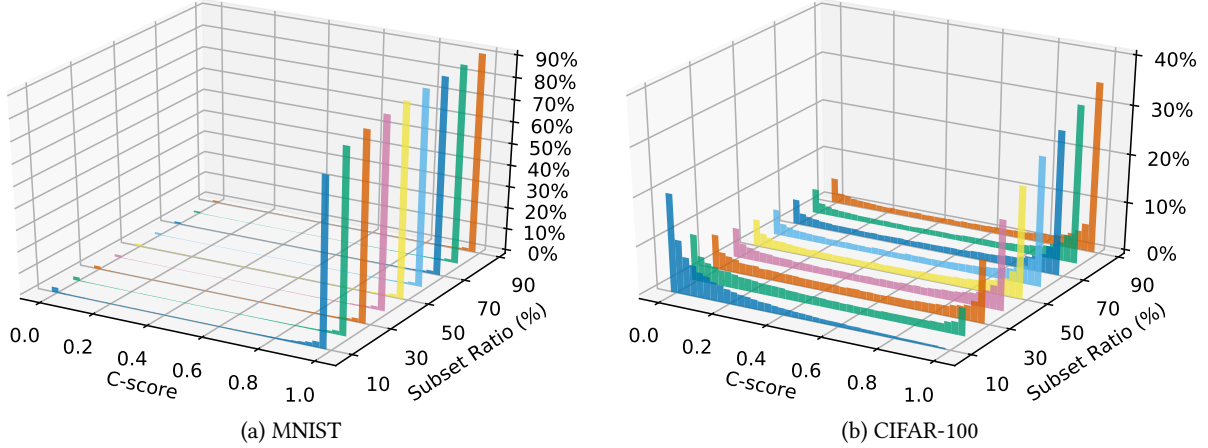


Figure 9: Histogram of C-scores for MNIST for subset ratios  $s \in \{10, 20, 30, \dots, 90\}$ . The vertical axis is the percentage of the 50,000 instances that fall into a bin.

computed on the gradient representations. We leave as future work to explore efficient algorithms to practically compute this score.

## D Point Estimation of Integral C-score

The histogram of individual point estimated C-scores with fixed subset ratios on CIFAR-10 is shown in Figure 2a. The same plot for MNIST and CIFAR-100 are shown in Figure 9.

Similarly, the histogram for the estimated integral C-scores for MNIST and CIFAR-100 are shown in Figure 10, which can be compared with the results for CIFAR-10 in Figure 2b in the main text.

## E Examples of Images Ranked by C-score

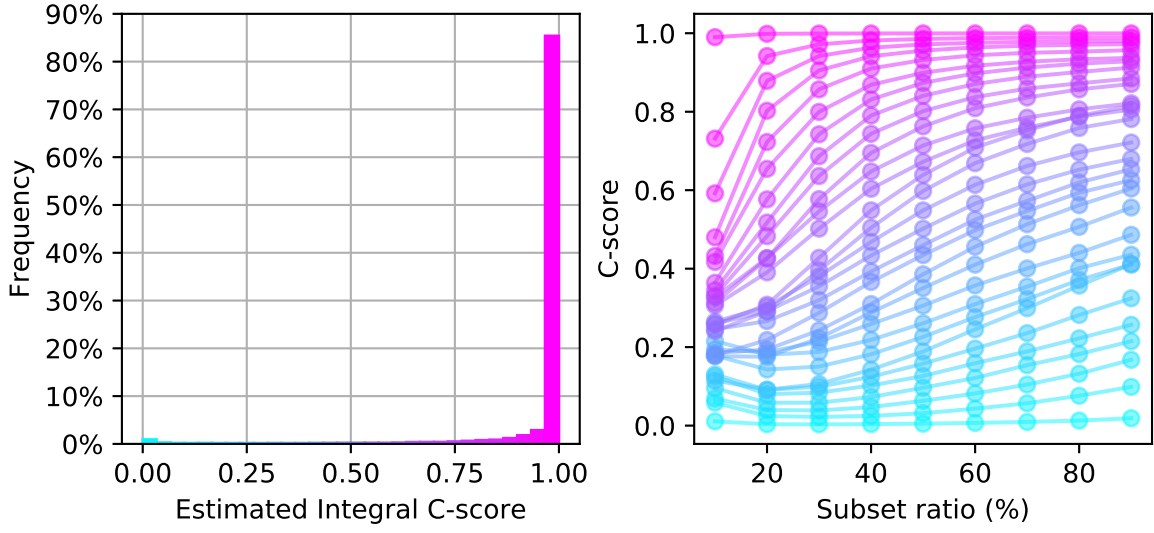
Examples with high, middle and low C-scores from a few representative classes of MNIST, CIFAR-10 and CIFAR-100 are show in Figure 3. In this appendix, we depict the results for all the 10 classes of MNIST and CIFAR-10 in Figure 11 and Figure 12, respectively. The results from the first 60 out of the 100 classes on CIFAR-100 is depicted in Figure 13.

## F What Makes an Item Regular or Irregular?

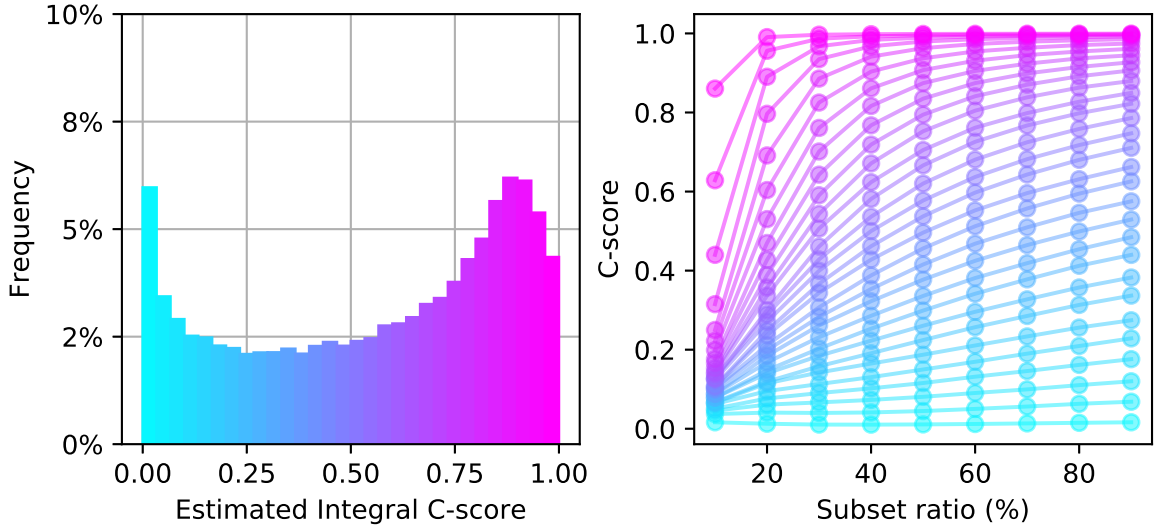
The notion of regularity is primarily coming from the statistical consistency of the example with the rest of the population, but less from the intrinsic structure of the example’s contents. To illustrate this, we refer back to the experiments in Section 4.2 on measuring the learning speed of groups of examples generated via equal partition on the C-score value range  $[0, 1]$ . As shown in Figure 2b, the distribution is uneven between high and low C-score values. As a result, the high C-score groups will have more examples than the low C-score groups. This agrees with the intuition that regularity arises from high probability masses.

To test whether an example with top-ranking C-score is still highly regular after the density of its neighborhood is reduced, we redo the experiment, but subsample each group to contain an equal number ( $\sim 400$ ) of examples. Then we run training on this new dataset and observe the learning speed in each (subsampled) group. The result is shown in Figure 14, which is to be compared with the results without group-size-equalizing in Figure 7a in the main text. The following observations can be made:

1. The learning curves for many of the groups start to overlap with each other.
2. The lower ranked groups now learns faster. For example, the lowest ranked group goes above 30% accuracy near epoch 50. In the original experiment (Figure 7a), this groups is still below 20% accuracy at epoch 50. The model is now learning with a much smaller dataset. Since the lower ranked examples



(a) MNIST



(b) CIFAR-100

Figure 10: (left) histogram of estimated integral C-scores; (right) C-scores by histogram bin as a function of subset ratio  $s$ .

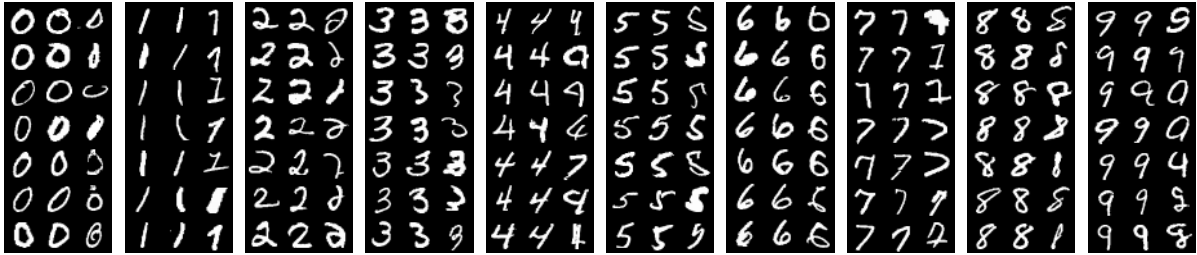


Figure 11: Examples from MNIST. Each block shows a single class; the left, middle, and right columns of a block depict instances with high, intermediate, and low C-scores, respectively.

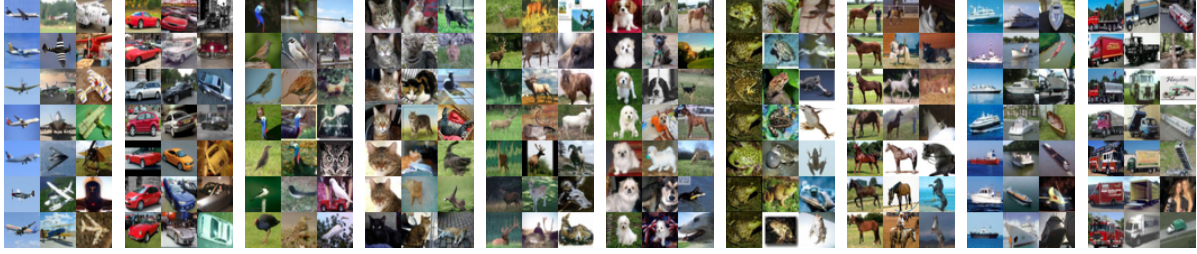


Figure 12: Examples from CIFAR-10. Each block shows a single class; the left, middle, and right columns of a block depict instances with high, intermediate, and low C-scores, respectively.

- are not highly consistent with the rest of the population, this means there are fewer “other examples” to compete with (i.e. those “other examples” will move the weights towards a direction that is less preferable for the lower ranked examples). As a result, the lower ranked groups can now learn faster.
3. On the other hand, the higher ranked groups now learn slower, which is clear from a direct comparison between Figure 7a and Figure 14. This is because for highly regular examples, reducing the dataset size means removing consistent examples — that is, there are now less “supporters” as oppose to less “competitors” in the case of lower ranked groups. As a result, the learn speed is now slower.
  4. Even though the learning curves are now overlapping, the highest ranked group and the lowest ranked group are still clearly separated. The potential reason is that while the lower ranked examples can be outliers in many different ways, the highest ranked examples are probably regular in a single (or very few) visual clusters (see the top ranked examples in Figure 3). As a result, the within group diversities of the highest ranked groups are still much smaller than the lowest ranked groups.

In summary, the regularity of an example arises from its consistency relation with the rest of the population. A regular example in isolation is no different to an outlier. Moreover, it is also not merely an intrinsic property of the data distribution, but is closely related to the model, loss function and learning algorithms. For example, while a picture with a red lake and a purple forest is likely to be considered an outlier in the usual sense, for a model that only uses grayscale information it could be highly regular.

## G Learning Rate Scheduling and Generalization

In Section 4.2 we used the C-score grouping to compare the learning dynamics of a stage-wise constant learning rate scheduler and a constant learning rate scheduler. The observations lead to an interesting hypothesis for explaining why stage-wise constant learning rate usually perform better and is preferred in many computer vision tasks. We provide more details here, and also compare to Adam, an optimizer with adaptive learning rate scheduling.

Figure 15 shows the learning speed of groups of examples on CIFAR-10 ranked by C-score, with SGD using stage-wise constant learning rate scheduling. This is the same as Figure 7a, replicated here for easy comparison. In Figure 16 we show the learning speeds of groups trained with SGD using constant learning rate scheduling. The 4 panels show the results for the each of the values used in the 4 stages of the stage-wise scheduler. In Figure 17 we also present the training results with the Adam optimizer, using the default base learning rate of 0.001. Adaptive algorithms like Adam scale the learning rate automatically and usually converge faster than vanilla SGD. However, it is observed that faster convergence from adaptive algorithms usually leads to worse generalization performances [26, 14, 17]. In fact, similar behaviors are observed, as summarized in Table 3.

To restate the hypothesis: the reason that stage-wise learning rate scheduler generalize better than others is that it delayed the memorization of outliers (low C-score examples) to later stages. In the first stage, when only the regular examples are learned, the patterns and structures discovered in those regular examples can be used to build a generalizable representation. In later stages, the memorization of outliers will not seriously disrupt the learned representation as the learning rate is much smaller than the earlier stages. In contrast, both Adam and SGD with (small) constant learning rate learn the outliers in parallel with the regularities, which may corrupt internal representations.

Our experiments are by no means extensive enough to fully verify this hypothesis. However, we think this is an very interesting side observation from our experiments that is worth mention. It also provide a concrete

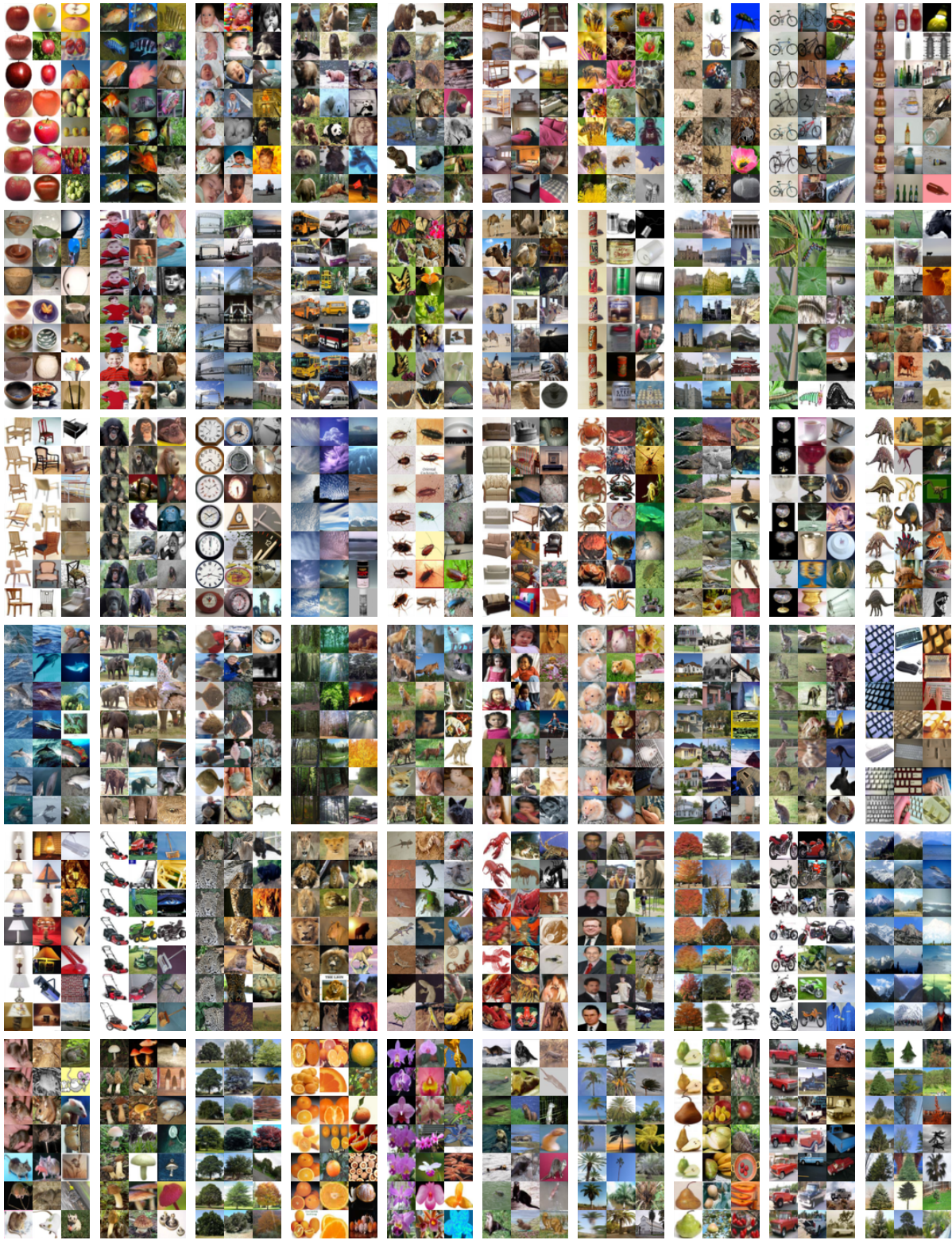


Figure 13: Examples from CIFAR-100. Each block shows a single class; the left, middle, and right columns of a block depict instances with high, intermediate, and low C-scores, respectively. The first 60 (out of the 100) classes are shown.

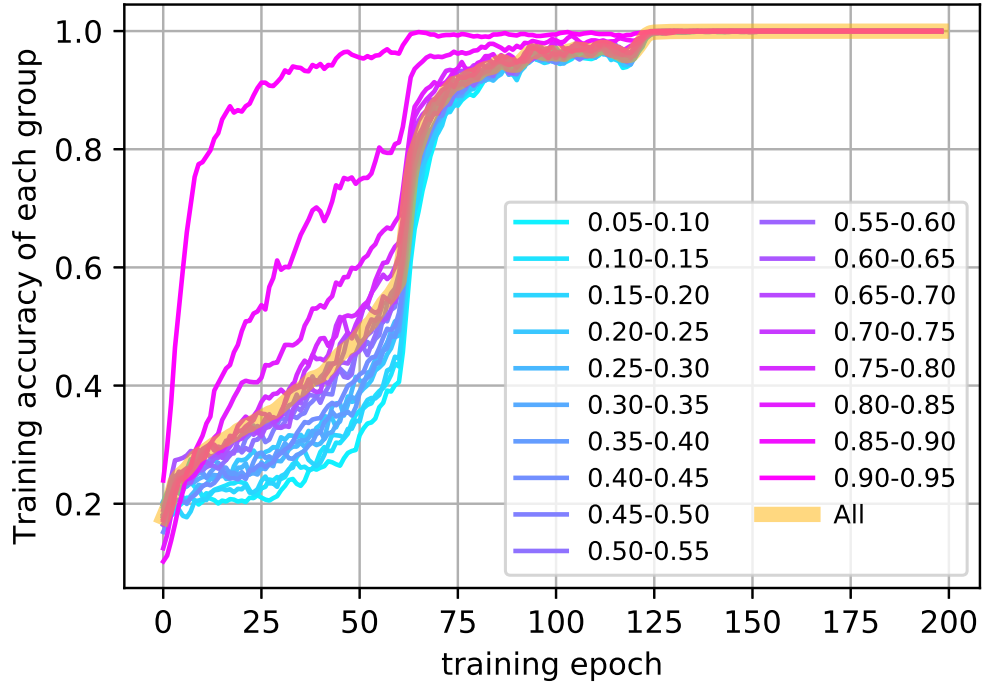


Figure 14: Learning speed of group of examples ranked by C-scores, with equal number (400) of examples in each group via subsampling.

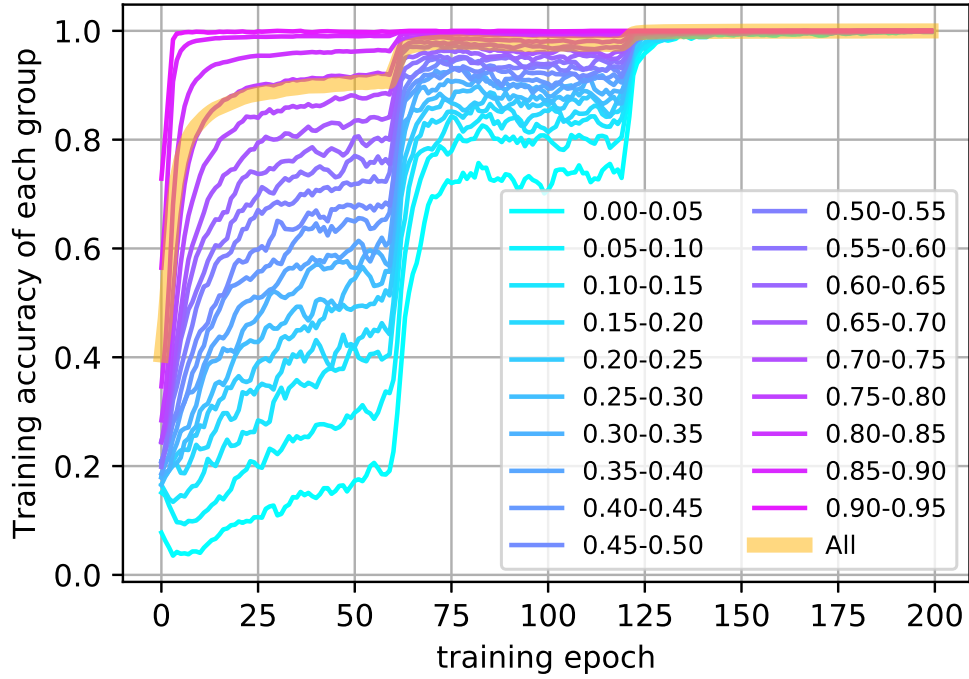


Figure 15: Learning speed of examples grouped by C-score with SGD using stage-wise constant learning rate.

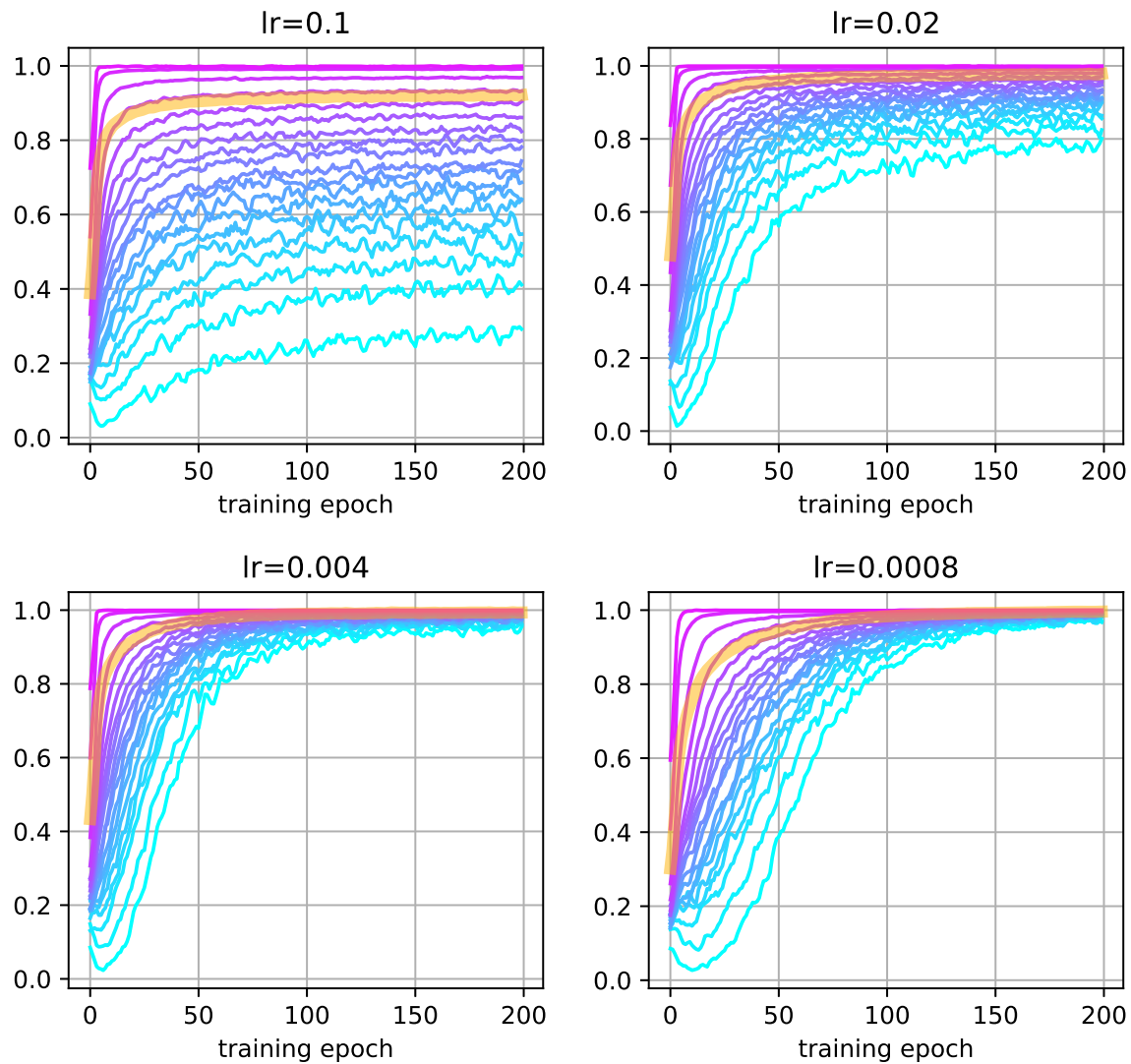


Figure 16: Learning speed of examples grouped by C-score with SGD using constant learning rate. The 4 different learning rates correspond to the constants used in the stage-wise scheduler in Figure 15.

Table 3: Test performance of models trained with various optimizers and learning rate schedulers on CIFAR-10.

Optimizer	Learning Rate	Test Accuracy (%)
SGD	Stage-wise	<b>95.14</b>
SGD	0.1	84.84
SGD	0.02	91.19
SGD	0.004	92.05
SGD	0.0008	90.82
Adam	Adaptive	92.97

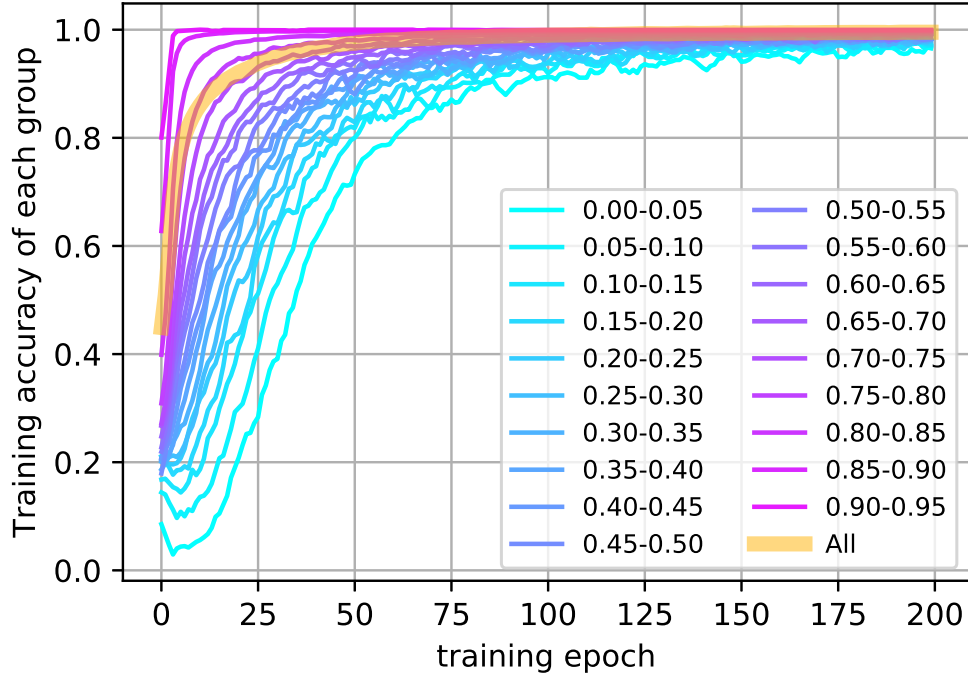


Figure 17: Learning speed of examples grouped by C-score with Adam optimizer.

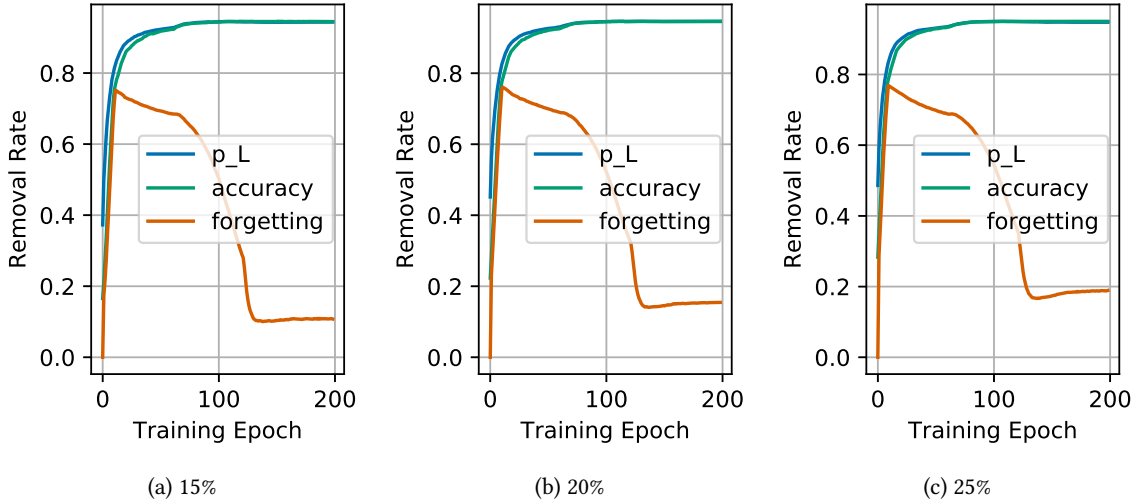


Figure 18: Experiments of outlier removal on CIFAR-10 where a (a) 15%, (b) 20%, and (c) 25% subset of the training set is corrupted with random label outliers.

example of how our C-score indexing could be useful for research topics on analyzing and understanding. We leave it as future work to systematically investigate the aforementioned hypothesis.

## H Code and Pre-computed C-scores

We provide code implementing our C-score estimation algorithms with a demo on MNIST, and pre-computed C-scores for CIFAR-10, CIFAR-100 and ImageNet (downloadable from <https://pluskid.github.io/structural-regularity/>). The exported files are in Numpy's data format saved via `numpy.savez`. For

CIFAR-10 and CIFAR-100, the exported file contains two arrays `labels` and `scores`. Both arrays are stored in the order of training examples as defined by the original datasets found at <https://www.cs.toronto.edu/~kriz/cifar.html>. The data loading tools provided in some deep learning library might not be following the original data example orders, so we provided the `labels` array for easy sanity check of the data ordering.

For ImageNet, since there is no well defined example ordering, we order the exported scores arbitrarily, while include the filename of each example to help identify the example-score mapping. More specifically, the exported file for ImageNet contains three arrays `labels`, `scores` and `filenames`. Again we include `labels` for easy sanity checking.